RAMAN AND BRILLOUIN SPECTROSCOPY IN A NEW LIGHT:

FULL BODY IMAGING OF DANIO RERIO EMBRYOS

An Undergraduate Research Scholars Thesis

by

JESSICA HANSON

Submitted to the Undergraduate Research Scholars program
Texas A&M University
in partial fulfillment of the requirements for the designation as an

UNDERGRADUATE RESEARCH SCHOLAR

Approved by
Research Advisor: Dr. Vladislav Yakovlev

May 2016

Major: Biomedical Engineering

TABLE OF CONTENTS

ABSTRACT

Raman and Brillouin Spectroscopy in a New Light:
Full Body Imaging of Danio Rerio Embryos

Jessica Hanson
Department of Biomedical Engineering
Texas A&M University

Research Advisor: Dr. Vladislav Yakovlev
Department of Biomedical Engineering

Biomechanics is a rapidly advancing field. Fundamental understanding of developing biological organisms on the microscopic level is one of the perspective directions of biomechanics research. Emerging technologies based on Raman and Brillouin spectroscopies are used to investigate the elastic and chemical properties of developing Zebrafish. Brillouin and Raman spectra were collected and analyzed from different parts of developing embryos, and this information was used to acquire two-dimensional images of live embryos at different stages of development. Since alternations in local chemical and viscoelastic properties can lead to potential diseases, this research in the future could be expanded to provide a better understanding of brain and heart development in order to prevent serious diseases.

CHAPTER I

INTRODUCTION

Biomechanics aids the development of biological organisms, and has an important role in the structure and function of biological systems [1,2]. Optical spectroscopic techniques have empowered biomedical researchers and engineers to investigate the elastic properties, a potential biomechanical property, of many materials. Elastography has commonly been used to map the elastic properties of tissues and cells in cancer and various diseases, muscles, cartilage, bone, and biomaterials [3]. Currently, elastography techniques are divided into two groups, macroscopic and microscopic techniques. Magnetic Resonance Imaging Elastography (MRIE) and ultrasound imaging are macroscopic techniques, while Atomic Force Microscopy (AFM) and optical tweezers are microscopic techniques. Macroscopic techniques are unable to investigate cellular/subcellular components. Whereas microscopic techniques are capable of making measurements at a cellular/subcellular level, but require mechanical contact or invasion, making them unsuitable for *in-vivo* studies [4]. Unfortunately, microscopic biomechanical properties of living organisms are not simply related to the macroscopic properties of the same material. The mechanical properties depend not only on discrete functions, but also the scale of measurement [5]. For example, type 1 collagen fibers have an elastic modulus of several GPa when measured using AFM, but macroscopic collagen tissues have a modulus of several kPa [5, 6]. Cancer cells are another excellent example. When measured using AFM cancer cells were softer than healthy cells [7, 8, 9], but they were more than 10 times stiffer than healthy tissues on a macroscopic level [10, 11]. In order to further understand the underlying mechanisms of biological systems, a spatial resolution of 100 nm to 10 μm, the typical size of a human cell, is required.

MRIE and ultrasound imaging are the most common macroscopic techniques. MRIE is capable of real-time whole body images with a relatively quick data acquisition speed [3], but its spatial resolution is more than 1 mm. Ultrasound has a better spatial resolution capable of greater than 50 μm imaging, but is limited by the diffractive nature of the acoustic wave and slower acquisition speeds [4]. AFM has the smallest spatial resolution but it is invasive. Optical tweezers provide the desired spatial resolution, 100 nm to 10 μm, but require mechanical perturbation of the sample, potentially altering it. Brillouin spectroscopy fills the technological gap, while Raman spectroscopy gives insight to the nature of the chemical bonds of the material. They have a spatial resolution of approximately 1 μm and an acquisition speed faster than AFM and optical tweezers [12]. Together, they also have the capability to image viscoelasticity, unlike any current optical technique. They are also noninvasive, nondestructive, and non-altering on the material of interest. [13, 14, 15, 16]

In Raman spectroscopy, the incident light from the laser beam interacts with the material's molecules. These molecules vibrate, rotate and deform naturally. The molecular deformations interact with the incident light causing a shift in the light. This shift depends on the pump laser frequency and the difference in energy between the molecules excited vibrational level and its grounds state. Each type of molecule has its own unique vibrational level. Its uniqueness allows Raman spectroscopy to identify the molecules found in a material [2].

Unlike Raman spectroscopy, Brillouin spectroscopy is able to characterize larger bulk changes in materials and is a technique based on the inelastic scattering of light in a material due to thermally excited acoustical phonons, not molecular deformations. Once the laser beam hits a material, the

incident phonons interact with the thermal phonons. As a result, the scattered light will experience a frequency shift. Brillouin spectroscopy is used to measure the frequency shift upon scattering. These changes directly relate to the sound speed in the material, which are closely related to the viscoelastic properties of the material. The following formula is for the Brillouin shift: $\nu_B = \pm 2\nu_L \frac{V}{c} \sin\frac{\theta}{2}$. Here, ν_L is the frequency of the incident light, $V = \sqrt{E/\rho}$ is the speed of sound in the material, E the elastic modulus (longitudinal modulus), ρ the mass density and θ the angle between the incident and the scattered light. As an optical technique Brillouin spectroscopy is compatible with many other optical techniques. In this particular set of experimental studies, it was coupled with Raman spectroscopy [2,12].

In this report, the application of Raman and Brillouin spectroscopies is expanded to include full body imaging of developing Danio rerio (Zebrafish) embryos during the first 48 hours of development. The Zebrafish model system has become increasingly popular in the biomedical field due to its overall optical transparency, the relatively quick speed of development, and its relatively similar genome and heart structure to humans. Recent studies of Zebrafish have primarily focused on the physical development of organisms through microscopic observations, mutated genes and their effects, and cardiac regrowth post-cardiac injury. Quantifying and understanding the viscoelastic properties of a developing embryo may open a new avenue in the study of disease progression and biological development.

CHAPTER II

MATERIALS AND METHODS

Raman and Brillouin spectrometer set up

Figure X(a) illustrates the experimental set up of the Raman and Brillouin spectrometers. A 532 nm single-frequency laser pump was used. Its center wavelength was specified as 531.9587 nm ± 0.3 pm. The pump had a maximum output power of approximately 100 mW and a nominal output line-width of 640 kHz. To prevent optical set up feedback an optical isolator was used to ensure the beam was transmitted in only one direction. A 20x objective lens (Nikon CFI Plan Fluor 20x) focused the laser beam on the specimen of interest and collected the backscattered light. The lens was manually adjusted along the optical axis to focus on the specimen. A translational XY stage (Micos Inc., model SMC MT-40 2D) was used to move the specimen laterally. A faraday optical rotator (FR) (ElectroOptics Technology, Inc.) was used to rotate the polarization of the backscattered light by 90°. The polarizing beam splitter (PBS) was placed in the beam path to direct backscattered light towards the Brillouin and Raman spectrometer. A 537.5nm long-pass filter (LP) was used to separate the Raman and Brillouin signals before the backscattered beam was sent to the Brillouin and Raman spectrometers. With the described setup the spatial resolution of the system was as small as 1.5 microns. However, the chosen step size of the stage, which was less than 25 microns, actually defined the image resolution. The pump power was always less than 70 mW, but usually less than 35 mW, to protect the embryo when focused at it during all measurements.

An optical microscope, also depicted in Figure 1, was used to position the laser beam focal spot. While the optical microscope was used a natural density filter was inserted in the laser beam path to prevent the laser from saturating the camera. The sample was then illuminated by an LED. The optical microscope image was collected with a CMOS camera (Mightex Inc., BCE-C050-U). The VIPA spectrometer, Figure 1, followed the design by Meng, et al. [12]. During the experiments, the morphology and integrity of the Zebrafish embryo was maintained.

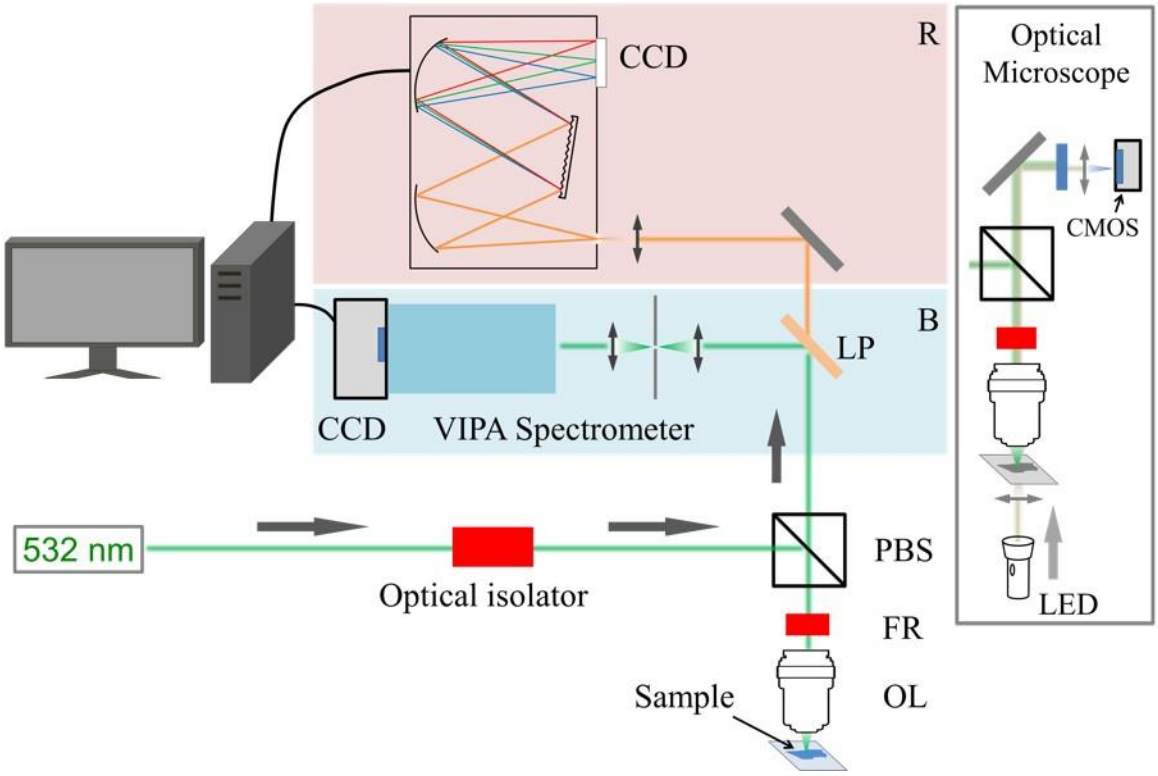

Figure 1: Raman and Brillouin Spectrometer Set Up

Zebrafish

IBC permit IBC2013-046 and AUP 2015-0083 were used to guide the experiments. Three types of Zebrafish were studied. The sp5mutEGFPcmlc2mRFP and the sp5lEGFPcmlc2mRFP Zebrafish were used due to the red fluorescence protein expressed in their heart, which ensured the laser was

focused on the heart during studies of heart elasticity. Wildtype Zebrafish was also used during the full body scans. The Zebrafish colonies were bred using specialized breeding tanks set up the afternoon before the breeding occurred. The specialized tanks consisted of a slotted bottom tank placed inside a slightly larger solid bottom tank. The slots allowed the embryos to fall into the large tank to be collected. A divider was used to separate the male and female until the time of breeding, usually between 8 am and 9 am. Once the divider was removed, the tanks were examined on 15-30 minute intervals to check for fertilized embryos. If embryos were discovered, they were collected and stored in a petri dish. Before being stored in an incubator at 28.5 degrees Celsius, the embryos were placed in a new petri dish filled with fresh fish water. No more than 50 embryos occupied a petri dish filled with fish water. Once the embryos were 10- 24 hours old they were moved into a petri dish containing 1x 1-phenyl 2-thiourea (PTU) in fish water. PTU was added to the fish water to inhibit the formation of melanophores and its effect of the conversion of tyrosine into melanin, ensuring the embryo remained transparent [17]. Until the embryos were used in the experiment, they remained stored in the incubator.

Before the embryos were mounted on a slide their chorions were removed and they were placed in a 1-2.5x solution of 2-amino benzoic acidethylester (Tricaine) for 5-10 minutes, in order to anesthetize them. After the administering of Tricaine, the embryo would remain still. During development the embryo usually twists its body. The embryo was mounted in 1.2% low-melt agarose in 1X fishwater on a glass slide. The Tricaine solution was also added on top of the agarose after it firmed around the embryo, ensuring the embryo remained anesthetized. After the needed data was collected from an embryo, it was euthanized in an ice water bath and stored in the freezer to await proper disposal.

Data processing

Both the Raman and Brillouin data were analyzed using MATLAB GUIs. To filter the noise the following methods were incorporated. Spectral averaging through the use of boxcar averaging was implemented first. A Gaussian curve was applied to fit the data to a specified curve. Spatial averaging was also used to filter the data by means of averaging the four immediate neighbors to the pixel. In this experiment the selected pixel was weighted 80% of the calculated total while the neighbors were weighted 5% each. Once spatial averaging was applied, the border pixels were removed since they lacked the appropriate surrounding pixels.

For Brillouin data, the most apparent elastic peak and anti-stokes peak of the data set were used to calculate the Brillouin shift. Bounds were selected to locate each peak's center. The center was located by fitting a Gaussian curve to the data, and finding the peak. To correlate peak location with frequency, the other four elastic peaks were located and matched to their known frequencies. A polynomial fit was used to interpolate across the spectral range. This data was used to convert peak location to frequency. The Brillouin shift was then calculated by subtracting the elastic peak frequency from the anti-stokes peak frequency. The Brillouin shift was then used to create a pixelated image of the zebrafish embryos.

For Raman data, the region of the Raman curve corresponding to organic contents was studied. The organic contents fell between locations 2800-3000 cm^{-1} (Pixels 720-790) of the data set. Before fitting a Gaussian curve to the data, the background was removed. Using the Gaussian fit, the peak amplitude, center, and width were calculated, along with the r-squared value of the fit.

Once the data was processed, four images were constructed to investigate the data. A pixel plot of peak amplitude, center, and width were created.

CHAPTER III

RESULTS AND DISCUSSION

Initial single point acquisitions were performed on Zebrafish embryos between 10 and 48 hours post fertilization. An example of the bright field microscope image is depicted in Figure 2(a). This image is of a Zebrafish embryo's eye and head region. On each acquisition day, a single embryo was randomly selected. Raman and Brillouin data was collected from the embryo in three locations: the eye, water, and yolk sac. These three locations are labeled in Figure 2(b). The Brillouin and Raman data are respectively illustrated in Figure 3(a) and Figure 3(b) [12].

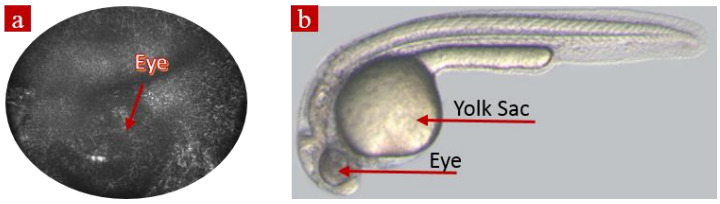

Figure 2: Zebrafish Embryo Images

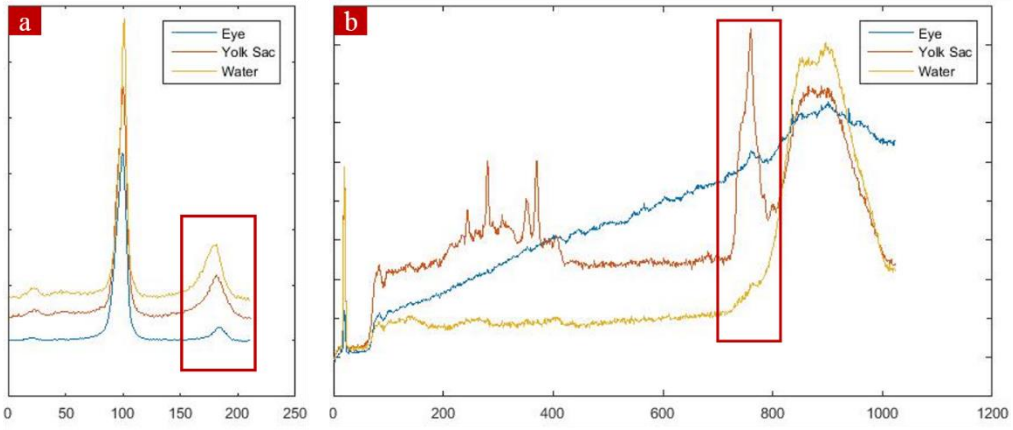

Figure 3: Brillouin (a) and Raman (b) Spectra

The Brillouin data in Figure 3(a) contains three peaks. The three peaks represent the Stokes (left) peak, the elastic (center) peak, and the anti-Stokes (right) peak. The elastic peak is caused by the elastic scattering process. The Stokes and anti-Stokes peaks result from the Brillouin scattering process. For this study only the anti-stokes (boxed peak) and elastic peak were used to calculate the Brillouin shift, because the absorption band of the iodine cell affected the shape of the Stokes peaks. A Gaussian curve was fitted to both peaks in order to find the Brillouin shifts. In figure 3(a) the blue data represents the Brillouin spectra acquired for a Zebrafish embryo's eye. The red line represents the Brillouin spectra for the embryo's yolk sac. The yellow line represents the water surrounding the embryo. The Brillouin shift for each line was calculated by locating the anti-Stokes and elastic peaks and converting pixel number (x-axis) to frequency in GHz. Using this system water, sampled from the water surrounding the embryo, has a Brillouin shift of 8.1-8.2 GHz. This reference value was used to calculate the Brillouin shifts of the eye and yolk sac, which were 8.4-8.5 GHz and 8.8-9 GHz respectively. In normal conditions the Brillouin shift for water is 7.46 GHz. The difference between this study and the previous reports may have resulted from the limited signal quality. Nevertheless, we have demonstrated that the Brillouin shift is sensitive to the probing position. In further studies our aim would be to improve the signal quality.

Due to the limited amplitude of the anti-stokes peaks the line widths of the peaks were not determined in this study. In future experiments, a 780 nm laser could be used to improve signal quality while further preventing thermal damage. A 780 nm laser, is within the 'biological window' which allows the power to be increased to compensate for limited signals [12].

Raman data is depicted in Figure 3(b). The entire Raman spectra was recorded for each point. The Raman data can be affected by embryo autofluorescence emissions and the glass slide's Raman/fluorescence emissions [12], thus elevating the Raman peaks. This study focused on the peak between 2800-3000 cm^{-1} (Pixels 720-790) in Figure 3(b) above (boxed data). This section of data corresponds to "organic contents"; vibrations of the chemical bonds between carbon and hydrogen, just as what is present in proteins and lipids [18]. The line colors correspond to the same parts of the embryo as for the Brillouin data. Blue represents eye, red represents yolk sac and yellow represents the water surrounding the embryo. The yolk sac has the highest peak in this reference area due to its larger content of CH_2/CH_3 bond vibration [19]. The eye's data set isincreasingly elevated due to its fluorescent properties.

The Brillouin shift and Raman peak height were also investigated two-dimensionally for developing embryos. To capture data at specified positions, a piezo xy translational stage was used. The z axis of the system was adjusted manually. Before obtaining the Raman and Brillouin data, microscope images were taken of the embryo. A step size and number of columns were selected. Then the stage was relocated to each position. An image was taken at each location using the microscope. The images were then assembled into whole images as Figure 4 demonstrates. The diameter of an embryo is approximately 0.88 mm [12]. Figure 5(a) illustrates the Raman data for the embryo used in Figure 4 using different colors to represent peak amplitudes between 2800-3000 cm^{-1}.

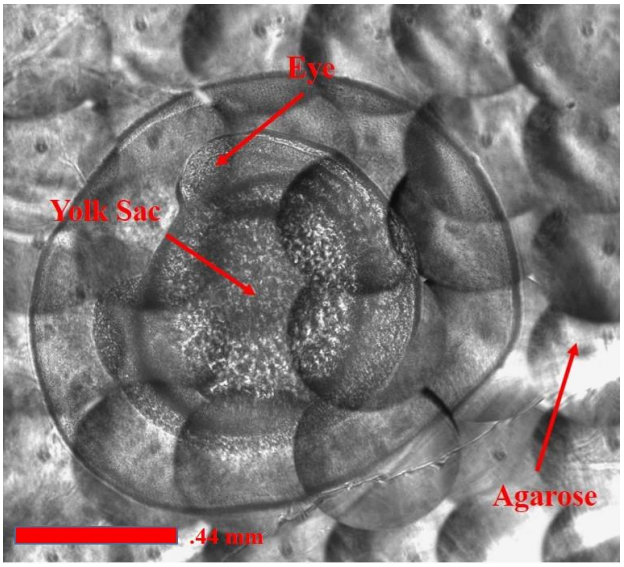

Figure 4: Compiled Zebrafish Embryo Image

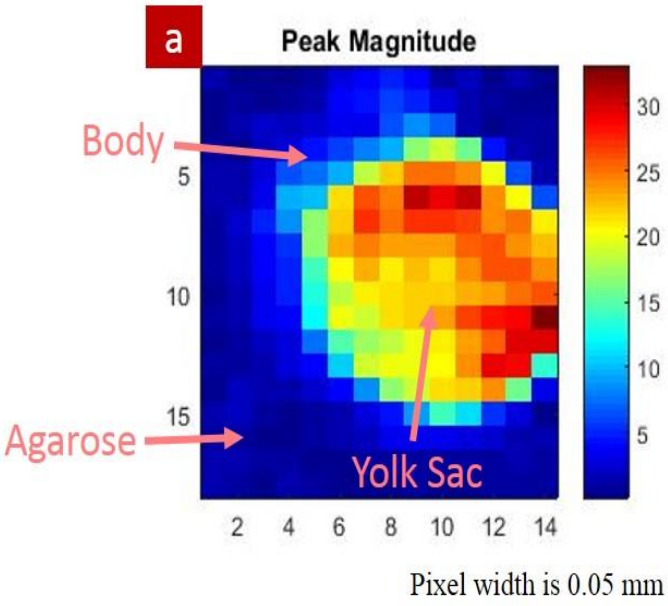

Figure 5: Raman Scan of Embryo 14 hours post fertilization

Compared to the surrounding medium of agarose (mainly water), the Zebrafish embryo gives more Raman scattering since it contains more organic components (Carbon-Hydrogen bonds). The Raman peak of the embryo will be less noisy than the agarose. Thus, we could better determine

the peak position for the pixels on the sample. Whereas, the Raman peak position for the agarose (surrounding medium) will be noisier/more inconsistent than the embryo.

Figure 6 is an image created with the Brillouin shifts of the embryo. The Brillouin shift of the image corresponds to the previously calculated values for water, and yolk sac. Unfortunately, the Brillouin data of the other scans had a low signal to noise ratio (SNR), thus not allowing the proper processing of any other scans due to the inability to locate the necessary peaks, even after filtering the data. In the future a low SNR could be rectified using a 780 nm pumping source due to a 'biological window'. Biological samples usually contain only two types of light absorbing molecules: water and biological pigment. Water is less absorbing of wavelengths of 460 nm, but is absorptive for wave lengths greater than 1000 nm (near infrared light). Whereas, most biological pigments, such as melanoma and hemoglobin, are less absorbent for infrared light and highly adsorbent for visible light (400-600 nm). However, at 700-900 nm wavelengths water and biological pigment absorption even out, so neither will be highly absorbent. When compared to the 532 nm wavelength, absorption at 780 nm wavelengths is reduced by approximately 100 times, thus, allowing the incident power to increase without thermally damaging the sample [20]. A higher incident power increases the signal while increasing the SNR. A higher SNR will allow better processing of the images by clearly defining the five reference elastic peaks and anti-Stokes peaks.

Another way to increase the SNR is through surface enhanced Brillouin spectroscopy and/or coherent/nonlinear Brillouin spectroscopy. Brillouin scattering can be enhanced if the sample is placed on an engineered metallic nanostructure [21]. Because the nanostructure may be too small

relative to the Zebrafish embryo it is less likely to be used in whole-body imaging applications. The Brillouin signal can be amplified using coherent/nonlinear optical processes including stimulated Brillouin spectroscopy and impulsive stimulated Brillouin spectroscopy [22]. By amplifying the signal, the peaks of interest will be easier to locate.

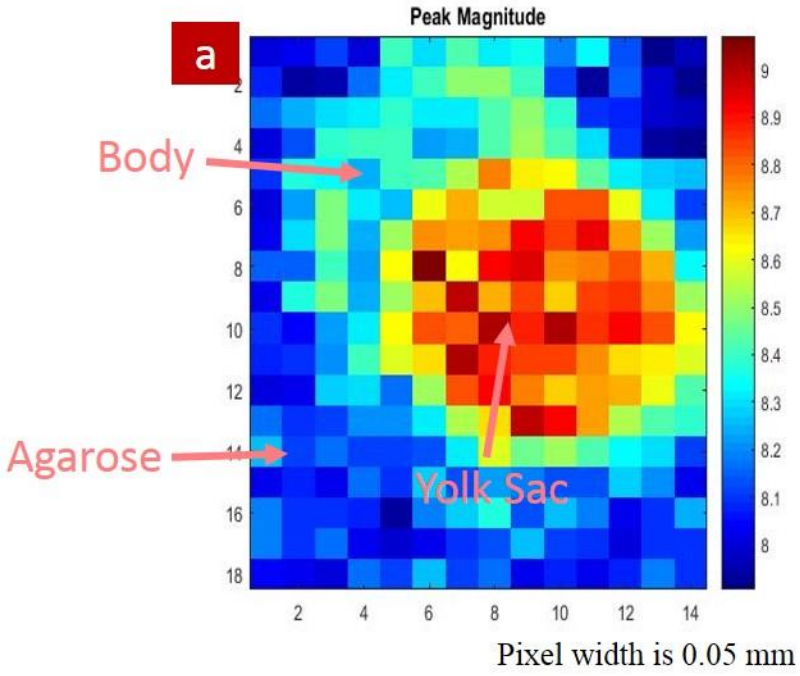

Figure 6: Brillouin image of 14 hour post fertilization Embryo

CHAPTER IV

CONCLUSION

This experiment proved that dual Raman and Brillouin spectroscopy can be used to investigate the elastic properties of a developing Zebrafish Embryo. It was discovered, the yolk sac of the embryo had the highest Brillouin shift, while the embryo body only had a slightly higher Brillouin shift and elasticity than water. This study also showed dual Brillouin and Raman spectroscopy can be used to create 2-D images of the of a Zebrafish embryo. In the future, dual Raman and Brillouin spectroscopy could be used to monitor the changes in properties as an embryo develops.

REFERENCES

[1] Yun, G. S. a. S. H. (2007). "Confocal Brillouin microscopy for three-dimensional mechanical imaging." nature photonics Vol 2(January 2008): 39-43.

[2] Andrew J. Traverso, J. V. T., Zachary A. Steelman, Zhaokai Meng, Marlan O. Scully, and Vladislav V. Yakovlev (2015). "A dual Raman-Brillouin microscope for chemical and mechanical characterization and imaging." Analytical Chemistry.

[3] Yogesh K Mariappan, K. J. G., and Richard L Ehman (2010). "Magnetic Resonance Elastography: A Review." Clin Anat(2010 July): 497-511.

[4] Nagy, K. C. N. a. A. (2008). "Single-molecule force spectroscopy: optical tweezers, magnetic tweezers and atomic force microscopy." Nat Methods(2008 June): 491-505.

[5] D.T. Butcher, T. A., and V.M. Weaver (2009). "A tense situation:forcing tumor progression." Nature Reviews Cancer 9(2): 108-122.

[6] G. Scarcelli, e. a. (2013). "Brillouin microscopy of collagen crosslinking: noncontact depth-dependent analysis of corneal elastic modulus." Investigative ophthalmology & visual science 54(2): 1418-1425.

[7] Suresh, S. (2007). "Biomechanics and biophysics of cancer cells." Acta Materialia 55(12): 3989-4014.

[8] S.E. Cross, e. a. (2007). "Nanomechanical analysis of cells from cancer patients." Nature nanotechnology 2(12): 780-783.

[9] J. Guck, e. a. (2005). "Optical Deformability as an Inherent Cell Marker for Testing Malignant Transformation and Metastatic Competence." Biophysical 88(5): 3689-3698.

[10] T.A. Krouskop, e. a. (1998). "Elastic moduli of breast and prostate tissues under compression. ." Ultrasonic imaging 20(4): 260-274.

[11] P. Wellman, e. a. (1999). "Breast tissue stiffness in compression is correlated to histological diagnosis." Harvard BioRobotics Laboratory Technical Report.

[12] Zhaokai Meng, S. C. B. L., Kenith E. Meissner, and Vladislav V. Yakovlev (2015). "Subcellular measurements of mechanical and chemical properties using dual Raman-Brillouin microspectroscopy." Journal of Biophotonics.

[13] Yun, G. S. a. S. H. (2007). "Confocal Brillouin microscopy for three-dimensional mechanical imaging." nature photonics 2(1): 39-43.

[14] O. Stachs, e. a. (2012). "Spatially-resolved Brillouin spectroscopy for in vivo determination of the biomechanical properties of crystalline lenses." Ophthalmic Technologies(Xxii).

[15] Yun, G. S. a. S. H. (2011). "Multistage VIPA etalons for high-extinction parallel Brillouin spectroscopy." Optics Express 19(11): 10913-10922.

[16] S. ReiB, e. a. (2011). "Spatially resolved Brillouin spectroscopy to determine the rheological properties of the eye lens." Biomedical optics express 2(8): 2144.

[17] Johnny Karlsson, J. v. H., and Per-Erik Olsson (2000). "Generating Transparent Zebrafish: A Refined Method to Improve Detection of Gene Expression During Embryonic Development." Marine Biotechnology 3(2001): 522-527.

[18] Charles B. Kimmel, W. W. B., Seth R. Kimmel, Bonnie Ullmann, and Thomas F. Schilling (1995). "Stages of Embryonic Development of the Zebrafish." Developmental Dynamics(203): 253-310.

[19] “Ana M. Herrero (2008) Raman Spectroscopy for Monitoring Protein Structure in Muscle Food Systems, Critical Reviews in Food Science and Nutrition, 48:6, 512-523“

[20] Weissleder, R., A clearer vision for in vivo imaging. Nature biotechnology, 2001. 19(4): p. 316-317

[21] Zhaokai Meng, V. V. Y., Zhandos Utegulov (2015). "Surface-enhanced Brillouin scattering in a vicinity of plasmonic gold nanostructures." Plasmonics in Biology and Medicine XII **9340**.

[22] Charles W. Ballmann, J. V. T., Andrew J. Traverso, Zhaokai Meng, Marlan O. Scully, Vladislav Yakovlev (2015). "Stimulated Brillouin Scattering Microscopic Imaging." Sci Rep(5).